

High-resolution reservoir characterization by an acoustic impedance inversion of a Tertiary deltaic clinof orm system in the North Sea

Daria Tetyukhina¹, Lucas J. van Vliet², Stefan M. Luthi¹, and Kees Wapenaar¹

ABSTRACT

Fluvio-deltaic sedimentary systems are of great interest for explorationists because they can form prolific hydrocarbon plays. However, they are also among the most complex and heterogeneous ones encountered in the subsurface, and potential reservoir units are often close to or below seismic resolution. For seismic inversion, it is therefore important to integrate the seismic data with higher resolution constraints obtained from well logs, whereby not only the acoustic properties are used but also the detailed layering characteristics. We have applied two inversion approaches for poststack, time-migrated seismic data to a clinof orm sequence in the North Sea. Both methods are recursive trace-based techniques that use well data as a priori constraints but differ in the way they incorporate structural information. One method uses a discrete layer model from the well that is propagated laterally along the clinof orm layers, which are modeled as sigmoids. The second method uses a constant sampling rate from the well data and uses horizontal and vertical regularization parameters for lateral propagation. The first method has a low level of parameterization embedded in a geologic framework and is computationally fast. The second method has a much higher degree of parameterization but is flexible enough to detect deviations in the geologic settings of the reservoir; however, there is no explicit geologic significance and the method is computationally much less efficient. Forward seismic modeling of the two inversion results indicates a good match of both methods with the actual seismic data.

INTRODUCTION

Inversion of seismic data is a widely used tool in the oil and gas industry for refining reservoir geometry and characterization. [Pendrel](#)

(2001) classifies seismic inversion methods based on the form of the objective function to be minimized. [Merletti and Torres-Verdin \(2006\)](#) divide all seismic inversion procedures reported in the open literature into two main categories: deterministic and stochastic methods. Geoscientists tend to use deterministic inversion methods as their first choice to characterize seismic data and to retrieve rock properties.

Due to the ill-posedness of the inverse problems, the solutions are not unique; i.e., a large number of solutions exist that satisfy the data within prescribed error bounds ([Cary and Chapman, 1988](#)). To find the best geophysical and geologic solution from the large number of available mathematical solutions, other conditions should be introduced ([Pendrel and Van Riel, 2000](#)).

Seismic inversion that uses Bayes's rule allows the information from all available measurements to be integrated into a consistent image of the reservoir and constrain these solutions based on a priori knowledge about the subsurface parameters. Prior knowledge (or prejudices) about the model parameters usually is combined with a "likelihood function," which depends on the misfit between the model response and the observed seismic data ([Duijndam, 1988a, 1988b; Treitel and Lines, 2001](#)).

The low vertical resolution of seismic data is the main motivation to integrate well log data into the inverse process and thereby complement the relatively dense horizontal coverage of seismic data with high-resolution borehole data ([Van Riel and Mesdag, 1988; Pendrel and Van Riel, 2000; Van Riel, 2000; Bosch et al., 2009](#)).

Another potential benefit of seismic inversion is the ability to incorporate structural and stratigraphic information of the reservoir to differentiate between similar mathematical solutions on the basis of their geologic viability ([Pendrel and Van Riel, 2000](#)). [Merletti and Torres-Verdin \(2006\)](#) perform an experiment in which they apply deterministic and stochastic prestack seismic inversion algorithms to characterize the complex progradation of a fluvio-deltaic sequence. They find that when seismic data does not permit estimation of the actual reservoir geometry, because of either its low vertical resolution or the high degree of facies amalgamation, the reliability of the

Manuscript received by the Editor 25 November 2009; revised manuscript received 9 June 2010; published online 20 December 2010.

¹Delft University of Technology, Department of Geotechnology, Delft, Netherlands. E-mail: d.tetyukhina@tudelft.nl; s.m.luthi@tudelft.nl; c.p.a.wapenaar@tudelft.nl.

²Delft University of Technology, Department of Imaging Science and Technology, Delft, Netherlands. E-mail: l.j.vanvliet@tudelft.nl.

© 2010 Society of Exploration Geophysicists. All rights reserved.

inversion result becomes increasingly dependent on a priori models as well as on the parameterization. In such cases, inversion loses its ability to narrow down the likely range of solutions in model space that simultaneously honor the seismic amplitude data and the well logs, thereby increasing the degree of nonuniqueness. The use of a priori models in close agreement with the stratigraphic framework thus effectively decreases the degree of nonuniqueness of inversion results (Merletti and Torres-Verdin, 2006).

The objective of this study is to develop a comprehensive, quantitative inversion method that allows high-resolution characterization of fluvio-deltaic sequences. Specifically, the study focuses on fluvio-deltaic clinoform systems, which are known to have complex internal lithofacies distributions that are difficult to image with the seismic method. However, these sedimentary systems often contain prolific oil and gas reservoirs, and their accurate characterization is therefore important in exploration and production.

In this study, two inversion methods that differ in the way they use stratigraphic constraints are developed and compared with each other. The novelty of the first method is that the seismic data and well logs are integrated with a stratigraphic model constructed with quantitative knowledge of the reservoir architecture. The innovation of the second method lies in its goal to adopt a “super-resolution” technique that favors sparse solutions for the clinoform characterization (Van Eekeren et al., 2010). Both inversion methods are not fully two-dimensional, but they are more than a series of independently processed 1D inversions. To stress the enforced continuity along the geologic structure, we use the name “pseudo-2D inversion.”

The potential benefits from these new approaches are that the implementation of the structural and the stratigraphic information accompanied by high vertical-resolution well data to the acoustic inversion technique considerably narrows the solution space of the inverse problem and increases confidence in the final result. The inversion methods were applied to a 3D seismic data set of an Upper Cenozoic fluvio-deltaic system in block F3 in the North Sea.

The paper is organized as follows. The North Sea field data set is described first. A detailed description of the two inversion methods is presented next, followed by a comparison of the results and then a discussion and conclusion.

FIELD DESCRIPTION

Geologic framework

The F3 block is located in the northeastern part of the Dutch sector of the North Sea. During the Cenozoic era, much of this region was characterized by a thermally subsiding epicontinental basin, most of

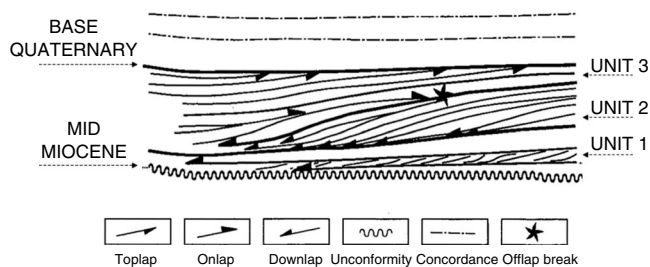


Figure 1. Sketch of the Neogene fluvio-deltaic system in the Southern North Sea. Modified from Steeghs et al. (2000).

which was confined by landmasses (Sørensen et al., 1997). During the Neogene, sedimentation rates exceeded the subsidence rate, and consequently shallowing of the basin occurred. A large fluvio-deltaic system dominated the basin, draining the Fennoscandian High and the Baltic Shield.

The Cenozoic succession can be subdivided into two main packages, separated by the Mid-Miocene Unconformity (Figure 1). The lower package consists mainly of relatively fine-grained aggradational Paleogene sediments (Steeeghs et al., 2000), whereas the package above consists of coarser grained Neogene sediments with much more complex geometries. Most of the above package is a progradational deltaic sequence that can be subdivided into three units, corresponding to three phases of delta evolution (Figure 1). The dominant direction of progradation is toward the west-southwest and is expressed as sigmoid lineaments (clinoforms) in the dip section (Tigrek, 1998). Unit 2, containing a conspicuous clinoform package, was chosen as the target zone for this study, and forms the delta foreset with a coarsening upward sequence. Its age is estimated as Early Pliocene. The coarse sediments are attributed to a regression caused by the Neogene uplift of Scandinavia in the Pliocene (Gregersen, 1997). Unit 2 becomes more sandy and silty in the basinward direction.

Data

A 3D seismic survey in block F3 covering an area of approximately 16×23 km² was acquired to explore for oil and gas in Upper Jurassic-Lower Cretaceous strata. It has become publicly available and accompanies a monograph by Aminzadeh and De Groot (2006). The seismic data are poststack, time-migrated data and therefore a function of two-way traveltime. A standard seismic data-processing sequence was applied to the raw data.

The data volume consists of 646 inlines and 947 crosslines. The line spacing is 25 m for both inlines and crosslines, and the sample rate is 4 ms. Well logs from four wells in the area are available, in particular sonic and gamma-ray logs. Density logs were reconstructed from the sonic logs using neural network techniques (Aminzadeh and De Groot, 2006). The selection of the seismic line to be characterized is based on the following criteria:

- 1) The target Unit 2 is present.
- 2) The seismic line contains Unit 2 along the progradational direction so that the clinoforms are well represented.
- 3) The internal layering of Unit 2 at the subseismic scale is present so that the high-resolution inversion technique can be tested.
- 4) A well is in the proximity so that a priori information can be obtained and inversion results can be validated.
- 5) The data are of good quality.

As a result, the seismic cross section displayed in Figure 2 was selected. Unit 2 has a time thickness of ± 230 ms and is fully penetrated by well F03-04, whose location is shown in Figure 2.

METHODS

The basic forward model used is a well-known 1D convolution model, in which transmission effects and multiples are neglected. The convolution in time is carried out as a multiplication in the frequency domain of the source wavelet's spectrum and the Fourier transform of the reflectivity time series. Under the assumption of

normal incidence of the downgoing waves on the reflectors, reflection coefficients are determined by the acoustic impedances.

As often is the case, the exact source wavelet was not available. Several methods exist for wavelet extraction from seismic data. The statistical extraction method used in estimating the wavelet assumes that the autocorrelation function of the wavelet is the same as the truncated autocorrelation function of the seismic trace. The average autocorrelation from several seismic traces is used, which strongly reduces noise and provides a more representative estimate when compared to a single trace procedure. The adoption of the convolution model implies assuming that the wavelet is time invariant, which is a reasonable assumption for a small target zone. Therefore, the seismic data cube was cropped to a subvolume of 100 inlines by 100 crosslines around the well in the lateral directions and from 665 to 894 ms (the target zone Unit 2) in the vertical direction (Petrel software by Schlumberger was used). The extracted wavelet is a zero-phase, symmetrical wavelet with a central frequency of 55 Hz. The length of the wavelet is 70 ms; the wavelet is shown in Figure 3a along with the wavelet spectrum in Figure 3b.

We used the P-wave velocity and density logs (recalculated from sonic logs) of the well F03-04 as the source of a priori information. To obtain usable amplitudes, the original well logs were first smoothed with a 2-m-long arithmetic, box-shaped filter along the entire length to reduce noise and remove spurious details (Figure 4). The sonic log was used to convert the well data from depth to time to relate the well data to the seismic. To extract as much a priori information as possible from the well data, an impedance log computed from the velocity and density logs served as the a priori mean vector.

One way to estimate parameter uncertainties when only a single well is available is to use a histogram of well measurements obtained from the target zone only. We used the standard deviation of the best-fit Gaussian distribution to the histogram of the acoustic impedance as the basis for the a priori covariance matrix. The possible correlations across different data points are ignored, and the estimated standard deviation is kept constant for all layers.

Similar to most inversion schemes, the procedure starts with an initial guess of the model parameters, from which an initial model response can be computed. Next the optimization algorithm yields a set of updated parameter estimates. These updated parameters are then “plugged” into the forward model (in our case, the convolution model), and the resulting new theoretical response produces an improved match to the data. We used a Levenberg-Marquardt optimization method, which is applied when the function to be minimized is a sum of squares. This corresponds to the maximum of the a posteriori probability under the assumption of additive Gaussian distributed noise on the observed data and Gaussian distributed priors. Moré (1978) gives a detailed description of this approach.

In the following sections, we present two pseudo-2D inversion methods to estimate the acoustic impedances in the clinoform sequence.

Method one: Stratigraphic model-based, low-parameterization seismic inversion

To obtain a 2D characterization of the clinoform sequence, three major steps are performed in method one. First, the thickness and acoustic impedance of the layers that compose the clino-

form package are estimated from well logs at a subseismic scale. Second, the entire clinoform is geometrically modeled based on seismic data, and its parameters are estimated. Third, the geometric models will guide the extrapolation of the a priori knowledge from the well to the next trace. This geometric model is used also to map the solution of the last processed trace to the initial guess of the next trace. In this manner, we characterize the complete 2D sequence.

1D inversion

The parameter vector to be estimated in the inversion procedure consists of the acoustic impedances and the time thicknesses of the layers.

As an initial model, we used a layered model at the location of the well (the “Well Model”); it is based on log analysis of the lithofacies and their layering.

The log interpretation is performed by comparing the gamma-ray log and P-wave velocity log. A basic rule for gamma-ray log interpretation is that lower values correlate with sandy layers and higher values correlate with the shale-rich layers (Luthi, 2001). Figure 5 shows a crossplot of the gamma-ray values against acoustic impedance values within the target zone; the color scale is assigned to the points as a function of depth to demonstrate the correlation between the two logs. There are two types of sediments that can be clearly distinguished from the plot: shale-rich sediments with generally higher gamma-ray values (bluish cloud, correlation coefficient 0.53) that belong to the upper part of the target zone (694–750 m) and sand-rich sediments with generally low gamma-ray values (reddish cloud, correlation coefficient 0.56) that belong to the lower part of the target zone (750–850 m). In addition, the compaction effect of the sediments can be observed because the deeper sediments on the plot are characterized generally by higher acoustic impedance values.

The constructed Well Model consists of 27 individual layers with typical thicknesses of 3 to 14 m and with lithologies presumed to alternate between shaly sands and sandy shales. The acoustic impedances of the Well Model were averaged within each layer. Because only layers located within half the wavelet’s length above or below the target zone have an impact on the seismic reflection, the transitions just below and above the target zone were included in the model.

The position of internal boundaries within the clinoform sequence can be quite ambiguous. Therefore, after the Well Model is established, it is iteratively refined by minimizing:

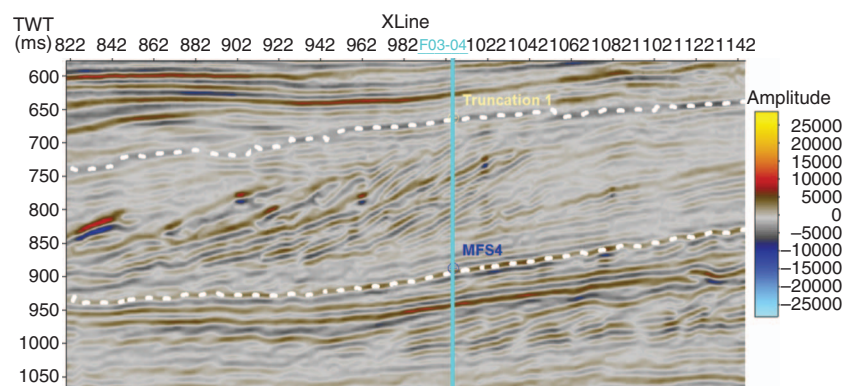


Figure 2. The seismic section (inline 441) chosen for the analysis and the location of well F03-04.

$$F(\mathbf{x}) = (\mathbf{y} - \mathbf{g}(\mathbf{x}))^T \mathbf{C}_n^{-1} (\mathbf{y} - \mathbf{g}(\mathbf{x})) + \lambda (\mathbf{x} - \hat{\mathbf{x}})^T \mathbf{C}_x^{-1} (\mathbf{x} - \hat{\mathbf{x}}), \tag{1}$$

where \mathbf{x} represents the model parameters, \mathbf{y} represents the poststack seismic reflection at the location of the well, $\mathbf{g}(\mathbf{x})$ represents the forward model based on 1D convolution with the estimated wavelet, \mathbf{C}_n represents the covariance matrix of the poststack seismic, λ represents the regularization parameter, $\hat{\mathbf{x}}$ represents the mean prior (coming from borehole data), and \mathbf{C}_x represents the covariance matrix of the parameters (the same covariance matrix for all seismic traces).

Estimation of the clinoform geometry

Once the parameters of the Well Model (i.e., the acoustic impedance and layer thickness) are estimated at the well location, the next step is to extrapolate this knowledge in the lateral direction along the clinoform package. For this, we first determine the clinoform shapes with the goal to parameterize them using a limited number of parameters (for our application, there are 10 unknown parameters in all). This set of parameters is used to analyze the morphology of the clinoform package and to characterize the clinoforms with incomplete information.

The advantage of this method is the small number of parameters that needs to be estimated. In addition, the geometric model might serve as a predictive tool for areas where the seismic resolution is too low to distinguish layers.

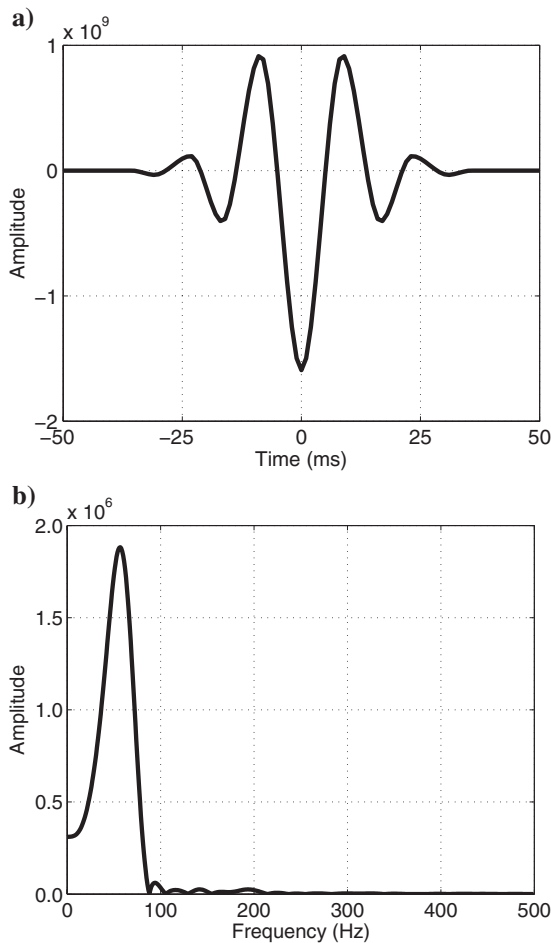


Figure 3. (a) The extracted wavelet and (b) its spectrum.

The stratigraphic signatures and stratal patterns in the sedimentary rock record are the result of the interaction of tectonics, eustasy, and climate. Tectonics and eustasy control the amount of space available for the sediment to accumulate (accommodation), and tectonics, eustasy, and climate interact to control sediment supply and how much of the accommodation is filled (Emery and Myers, 1996). Clinoforms are a common feature in a basin-margin setting and often have relatively flat topsets, followed by a distinct slope and relatively flat bottomsets (Figure 6).

Clinoforms develop typically at the front of river deltas or in subaqueous deltas. Subaqueous deltas are characterized by an overall sigmoid geometry in sections perpendicular to the shore, submerged offlap break (and lack of subaerial exposure of the topset), muddy lithology, and high sediment-accumulation rates (Cattaneo et al., 2003). Changes in clinoform thickness, internal geometry, and style of superposition of multiple clinoforms provide information regarding long-term margin subsidence, sea-level change, and short-term

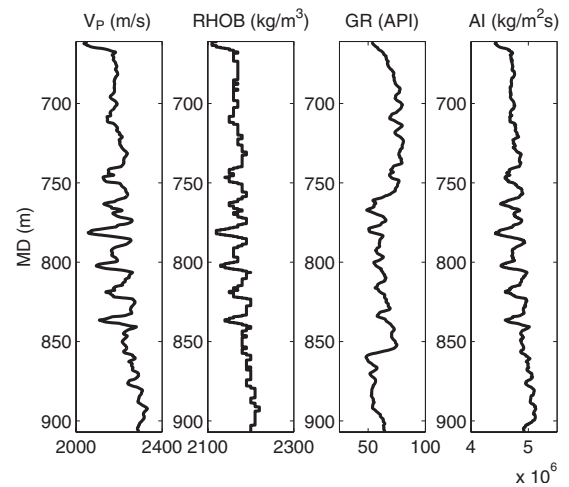


Figure 4. The P-wave velocity log (V_p), density log ($RHOB$, recalculated from the sonic log), gamma-ray log (GR), and acoustic impedance log (AI) of the well F03-04 (MD is measured depth).

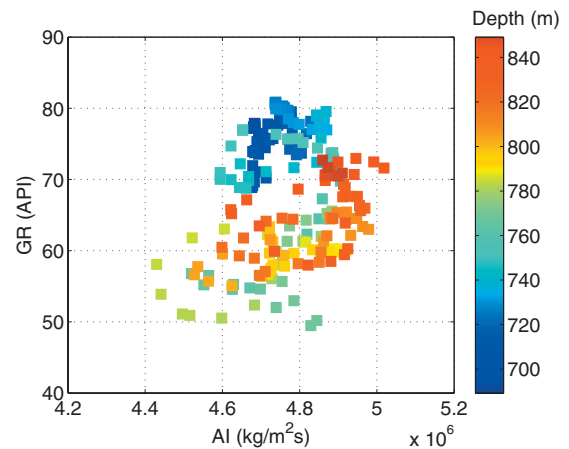


Figure 5. A crossplot of the gamma-ray values against acoustic impedance values within the target zone; the color scale is assigned to the points as a function of depth (in meters). See text for discussion.

fluctuations of sediment supply (Cattaneo et al., 2004). Three main growth patterns can be distinguished in clinoforms based on the rate of deposition and subsidence (Figure 6).

The F3 data set offers a good opportunity to develop models for high-resolution characterization of clinoform sequences because it contains large-scale sigmoid bedding as well as subseismic internal layering in Unit 2 as evidenced from the Well Model. Analysis of the clinoform zone displayed in Figure 2 shows that a combination of progradation and aggradation took place. Progradational geometries occur when the sediment supply exceeds the rate of the creation of topset accommodation and facies belts migrate basinward. On seismic data, progradation is expressed by clinoforms that show the basinward migration of the offlap break. Aggradational geometries occur when the sediment supply and rate of the creation of topset accommodation are roughly balanced. Facies belts stack vertically, and the offlap break does not migrate landward or basinward (Emery and Myers, 1996).

From a geometric point of view, a clinoform sequence can be approximated by a set of translated sigmoid curves. A sigmoid function $f_j(X)$ can be described by four parameters:

$$f_j(X) = c_j + \frac{b_j}{1 + e^{-(X-d_j)/a_j}}, \quad (2)$$

where a_j is a lateral scaling, b_j is a depth scaling, c_j is a depth offset, d_j is a lateral translation, and the index j identifies the clinoform in a sequence.

The next step is to relate the mathematical parameters with geologic processes. Based on the clinoform section, the progradation can be associated with the lateral translation parameter and the aggradation with the depth offset. Geologic objects are not random structures but follow typical patterns caused by the depositional processes that formed them. Here we presume that for every subsequent clinoform within the fluvio-deltaic system, the lateral and the depth scaling parameters stay approximately constant. On the other hand, the depth offset (aggradation) fluctuates slightly and the lateral translation (progradation) varies strongly. As a result, the whole clinoform sequence can be modeled by means of a parameter vector constructed by consecutive series of constant parameters (a and b) followed by varying parameters (c_j and d_j) for every layer.

The seismic objects extracted from the Unit 2 data set are partially eroded or otherwise affected by postdepositional processes. In addition, at the topsets and bottomsets the layers are thin and often poorly resolved on seismic images, leading to tuning effects. Initial parameters describing the sigmoid functions of the sequence were estimated from the seismic section by visual interpretation of the geologic sequence.

Special attention was paid to the lateral translation parameter d_j , which varies from one clinoform to the next. We introduced a lateral shift Δd_j to the initial model for every subsequent curve; Δd_j is equal to a small fraction of the length of the clinoform. The objective (cost) function to be minimized is represented by the sum of the individual objective functions for every clinoform in the package. Each objective function is represented by a likelihood function only, due to the absence of data-independent a priori information.

Inversion of the clinoforms

The inversion of a seismic section is done trace by trace; the technique is the same for each trace and is described previously. A central issue of method one is the incorporation of the structural information

into the inversion process in the form of a mathematical description of the clinoform shapes. These shapes are used to steer the trace inversion along the sequence, i.e., they serve as hard constraints (two-way traveltimes versus x -coordinates). Analogous to the 1D case, the well log data are used as a priori information.

The inversion process starts from the trace closest to the well. In this case, the Well Model again can serve as an initial model.

For the sake of convenience, we assume that the number of layers (defined in the Well Model) between two hard boundaries (clinoform layers) is kept constant throughout the entire sequence. Once the first trace is inverted, the estimated acoustic parameters are used as an initial model for the next trace. In addition, structural information retrieved from the modeled clinoform shapes provides knowledge about the trace-to-trace variation. Because the time thickness between clinoform layers — the hard constraints — varies from trace to trace (the distance is 25 m), a normalization factor is applied to adjust the initial model for the next trace by stretching or compressing. The normalization factor is defined by the ratio of the time lapse between the estimated shapes (hard constraint) of the current seismic trace and the previous seismic trace.

Method two: Grid-based seismic inversion

The assumption made in method one regarding a constant number of layers in the Well Model is a limitation. It does not allow for layers to appear or disappear along the clinoform sequence. Observation of the seismic data set shows that this assumption is valid in some parts of the sequence but not in others. Method two overcomes this problem by abandoning the explicit layer model of method one. Again a trace-by-trace inversion is applied, starting from the well, across the 2D clinoform sequence. All acquisition parameters (including the extracted wavelet) are kept the same as in method one. The well data remain the source of a priori information, but in a different representation.

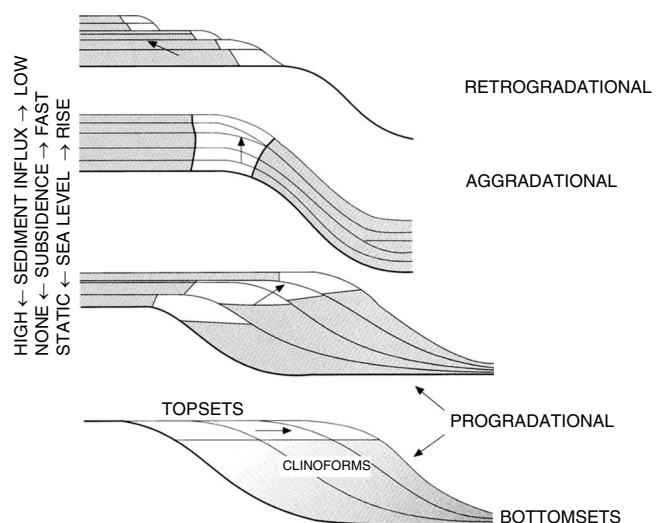


Figure 6. Depositional architecture of clinoforms as a function of the accommodation volume and sediment supply, with a typical profile comprising topsets, clinoform foresets, and bottomsets. Modified from Emery and Myers (1996).

To enforce a sparse solution, we adopted a method by Van Eekeren et al. (2010) that was successfully applied to obtain superresolution reconstruction of small moving objects. This method differs from the well-known sparse-spike acoustic inversion algorithms (Pendrel and van Riel, 1997; Debye and Van Riel, 1999) in the sparsity promoting factor used. Instead of commonly used techniques such as L_p deconvolution (Debye and Van Riel, 1999), mixed norms methods (Alliney and Ruzinsky, 1994), Cauchy criterion (Amundsen, 1991), Sech criterion (Cruse et al., 1990), Huber criterion (Huber, 1981), and the like, we used a total variation (TV) criterion, which is a modified L_1 -norm (Rudin et al., 1992; Li and Santosa, 1996; Farsiu et al., 2004). The norm provides excellent constraints (a priori knowledge) for problems with sparse solutions.

The method uses the same data misfit term as in equation 1 but uses regularization terms that favor sparse solutions, i.e., solutions for which $\|\nabla \mathbf{x}\| \cong 0$ holds for the majority of samples. The regularization within one trace is performed by the vertical operator (discussed below). This vertical operator (also discussed below) favors a sparse inversion solution. The horizontal operator favors continuity of the 2D inversion results and supports extrapolation of the well data along the sequence.

It should be noted that the structural information (estimated clinoform shape) is no longer used explicitly in this method, but is provided implicitly by the vertical and the horizontal operators.

1D inversion

A significant difference between methods one and two is that method one creates an initial well model for 1D inversion based on a lithofacies analysis of the well logs, whereas in method two the well impedance data are resampled with a constant time step. Every seismic trace is subsampled with the same time step.

The sampling time step is a user-specified parameter that reflects the desired resolution of the solution. For our application, a sampling step of 1 ms was chosen. An initial model for the current trace is the resulting estimate of the previously inverted trace. Due to a constant sampling step of the traces, no separate normalization is needed. The parameter vector to be estimated is constructed by the acoustic impedances as the amplitudes of the samples only.

The first additional term is the sum of absolute differences between adjacent samples in the solution vector of the trace and is further referred to as the “vertical operator.” This term favors solutions in which the sum of gradient magnitudes is small; these are called “sparse solutions.” The L_1 -norm is favoring a sparse solution, and for our application it minimizes the number of inverted layers by penalizing absolute differences between adjacent samples. Layers are no longer modeled explicitly but must show up in the resulting trace by the fact that the output of adjacent samples should be similar, except at layer boundaries. The trace sampling should be such that we assume many samples inside a single layer; i.e., the number of layers per trace is much smaller than the number of samples.

The minimization is done in an iterative way using the Levenberg-Marquardt method, which assumes that the cost function has first and second derivatives that exist everywhere. However, the L_1 -norm does not satisfy this assumption. Therefore, we use a hyperbolic norm as introduced by Van Eekeren et al. (2010),

$$\|\mathbf{x}\|_H = \sum_i (\sqrt{x_i^2 + \alpha^2} - \alpha), \quad (3)$$

where x_i represents the elements of \mathbf{x} .

The hyperbolic norm has the same properties as the L_1 -norm for large values ($x_i \gg \alpha$), and it has a first and a second derivative that exists everywhere. The values of acoustic impedances to be estimated, \mathbf{x} , are much larger than 1. Hence, by setting α equal to 1, the hyperbolic norm has the same properties as the L_1 -norm.

The model parameters are found by minimizing:

$$F(\mathbf{x}) = (\mathbf{y} - \mathbf{g}(\mathbf{x}))^T \mathbf{C}_n^{-1} (\mathbf{y} - \mathbf{g}(\mathbf{x})) + \lambda (\mathbf{x} - \hat{\mathbf{x}})^T \mathbf{C}_x^{-1} (\mathbf{x} - \hat{\mathbf{x}}) + \mu \sum_j (\sqrt{(x_j - x_{j-1})^2 + 1} - 1), \quad (4)$$

where j is a sample number, and \mathbf{x} is the vector of acoustic impedances that we are looking for.

As described above, the layering is controlled by the vertical operator that favors sparse solutions, meaning that the acoustic impedances that have similar properties are clustered together, thereby forming a “layer.” Consequently, the layering shows as series of maxima and minima on the estimated impedance curve. Estimating the number of layers therefore comes down to counting the number of sign changes when subtracting two successive impedance values.

Inversion of the clinoforms

The second additional term is a sum of absolute differences between lateral neighboring samples in the current (m) and the previous ($m - 1$) seismic trace, further referred to as the “horizontal operator.” This term accomplishes two tasks at once. First, it favors continuity of the inversion results along the clinoform sequence. Second, it extrapolates the a priori knowledge from the well to the current trace. Based on the above-mentioned consideration, a hyperbolic norm instead of the L_1 -norm is used.

The original second term in the cost function, which is the weighted L_2 -norm of the deviations of the parameters from their a priori mean values, can be omitted starting with the second seismic trace from the well because the horizontal operator extrapolates the well data to the current trace accordingly and takes lateral variations of the impedances along the sequence into account at the same time. The functional to be minimized is

$$F(\mathbf{x}^m) = (\mathbf{y}^m - \mathbf{g}(\mathbf{x}^m))^T \mathbf{C}_n^{-1} (\mathbf{y}^m - \mathbf{g}(\mathbf{x}^m)) + \mu \sum_j (\sqrt{(x_j^m - x_{j-1}^m)^2 + 1} - 1) + \gamma \sum_j (\sqrt{(x_j^m - x_j^{m-1})^2 + 1} - 1), \quad (5)$$

where $m > 1$ is a trace number.

Regularization

Minimization of the cost function is an ill-posed problem, and therefore regularization needs to be applied. A central issue in this section is how to select the weighting coefficients λ , μ and γ in front of the terms.

The parameter λ sets the balance between the data misfit and the a priori information and solution misfit. Although this term is used in the inversion of the first trace only, it still plays an important role in transferring the well data into the entire sequence.

The weighting coefficient μ in front of the vertical operator term restricts the amount of layers in the inverted trace. It penalizes small

fluctuations in the trace and yields “abrupt” changes between otherwise “smooth” layers.

The weighting coefficient γ in front of the horizontal operator term enforces lateral continuity of the impedances. In other words, it controls the number of fluctuations in the strata that can be interpreted from the resulting impedance model of the clinoform sequence.

To select the optimal combinations of the regularization parameters, first the 1D and pseudo-2D sensitivity tests were performed. The tests aided understanding the dependence on the parameters and thereby assisted in guiding the search for the optimum values. The second step uses the expertise of a geologist who can choose the most realistic solution, from a geologic perspective, from the selected group of the potential optimal regularization combinations. Based on this approach, the following combination of the regularization parameters was chosen as optimal: method one ($\lambda = 0.3$), method two ($\lambda = 1, \mu = 4, \gamma = 1$).

RESULTS

The results of our inversion methods are presented in the following order: first the comparison of the outcome of 1D seismic inversion (trace closest to the well location) of both methods, next the results of 2D clinoform estimation of the first method, and finally the comparison of the results of both methods. For the last test, we have selected the seismic section on the left-hand side of the well, consisting of 70 seismic traces.

Results of 1D inversion

Figure 7a and b illustrates the difference between the initial model (green, the manually interpreted Well Model for method one) and the estimated model (red) for the first method and the second method, respectively. Both models for each method are superimposed on the actual impedance log (blue). The estimated impedance in method one (Figure 7a) shows a good correlation with the well data, although it has a blocky structure except for the last part, which was not modeled explicitly (two-way traveltimes [TWT] 866–894 ms). The estimated impedance in the second method (Figure 7b) depicts a good correlation with the well data also. The vertical resolutions of the methods are high and lie beyond the seismic resolution; layers with thicknesses of as much as one tenth of the wavelength are well resolved close to the well location. The black arrows in Figure 7a and b indicate places where the methods show new information below the seismic resolution.

Figure 7c and d demonstrates the comparison of traces of the synthetic seismic based on the initial model (green, based on the manually interpreted Well Model for method one), the seismic based on the estimated model (red), and the actual seismic data (blue). Both methods yield a good match, except for the part that was not modeled explicitly in method one (TWT 866–894 ms).

Results of the clinoform geometry modeling

Four clinoform curves were selected for 2D inversion. The resulting geometries superimposed on the seismic image are depicted in Figure 8 (dashed lines), along with semiautomated trace picks (solid lines). It can be seen that the clinoform shapes were estimated quite accurately, and the measurements are summarized in Table 1. These were obtained from the estimated sigmoid parameters, namely, the lateral translation d_j and the depth offset c_j , which are associated with progradation and aggradation, respectively.

From Table 1, it is obvious that both aggradation and progradation occurred at variable rates and that progradation was the dominant process. Enlarged versions of the bottomset and the topset of the clinoform layers are depicted on Figure 9a and b, respectively. The black arrows indicate areas where the clinoform layers converge to such an extent that inversion is possible only through guidance by the sigmoid model (dashed lines) and where the inversion procedure has the capability to achieve a subseismic resolution.

Inversion results of the clinoforms

The estimated impedance models of the selected 2D seismic section using both methods are shown in Figure 10a and b, respectively. It should be noted that the structural information was incorporated explicitly only between four selected clinoforms, not in the entire target zone.

The result from the second method reveals a higher degree of lateral continuity of the impedance properties along the sequence. The estimated impedances (layered model) in method one follow quite well the shape of the initial sigmoid model as depicted in Figure 8.

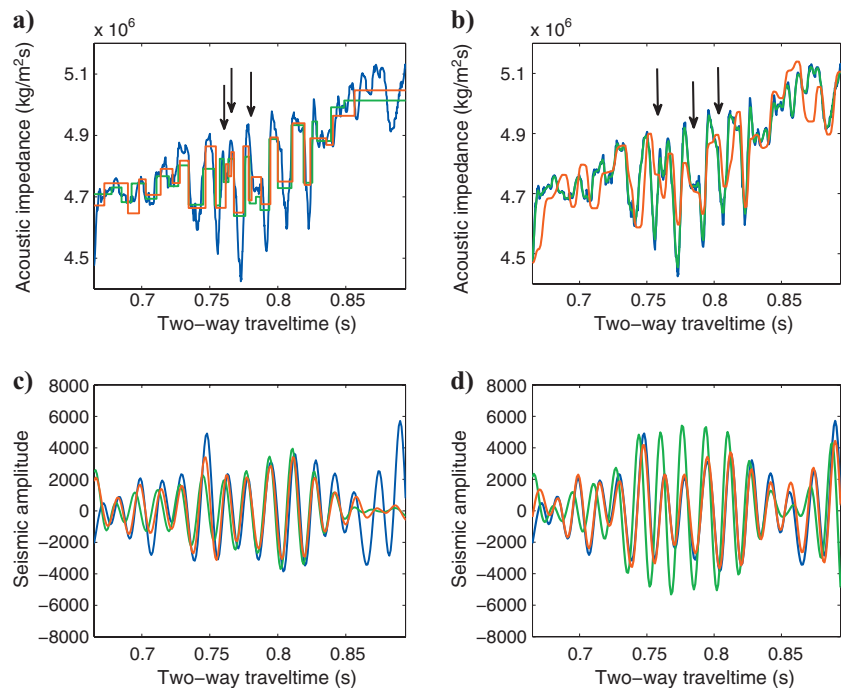


Figure 7. Results of the 1D inversion for method one (left column) and method two (right column): (a, b) initial models (green, Well Model for method one) and the estimated models (red) superimposed on the actual impedance log (blue); (c, d) comparison of the synthetic seismic trace based on the initial model (green, Well Model for method one), the seismic trace based on the estimated model (red), and the actual seismic trace (blue).

Figure 8. Models of four clinoform layers (dashed) that were estimated in method one are superimposed on the seismic image, along with semiautomated trace picks (solid lines). Black rectangles refer to Figure 9.

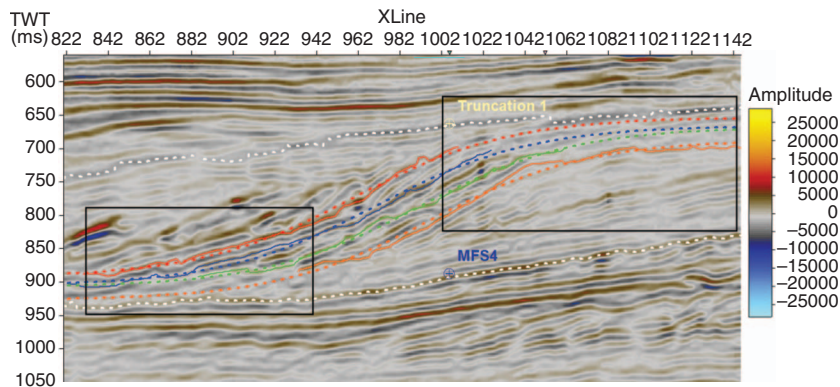


Table 1. Estimated values for progradation and aggradation rates obtained by fitting the sigmoid model to the semiautomated trace picks from the target zone.

Aggradation		Progradation	
Depth offset	Value (m)	Lateral translation	Value (m)
c_1	650	d_1	0
c_2	670	d_2	260
c_3	670	d_3	770
c_4	690	d_4	910

The simulated seismic sections based upon the estimated impedances of Figure 10a and b are displayed in Figure 11a and b, respectively. These figures illustrate that the second method gives a slightly better match with the seismic (blank areas in the first method were not modeled). For easier comparison, the actual seismic section is displayed in Figure 11c.

In Figure 12, we show the number of layers identified by the second method throughout the sequence. The number of strata that can be interpreted from the result fluctuates along the sequence, with the average number of layers, marked by the dashed line, being about 35. This result correlates with the manual interpretation of log data in method one (Well Model), but the average number of layers is slightly higher than the one estimated in method one (27 layers). The reason is that in the first method, the number of layers between the hard boundaries (Unit 2 boundaries along with the estimated clinoform shapes) was kept fixed. Hence, the difference in the average number of estimated layers for both methods is mainly due to the layers situated between the upper boundary of the target Unit 2 (white dashed line) and the first estimated clinoform (red dashed line) depicted in Figure 8. These layers were not modeled explicitly in method one.

DISCUSSION

The impedance model obtained from the first inversion method can provide valuable quantitative information about changes in reservoir quality across the field, but the second method provides more accurate quantitative information about the reservoir. According to

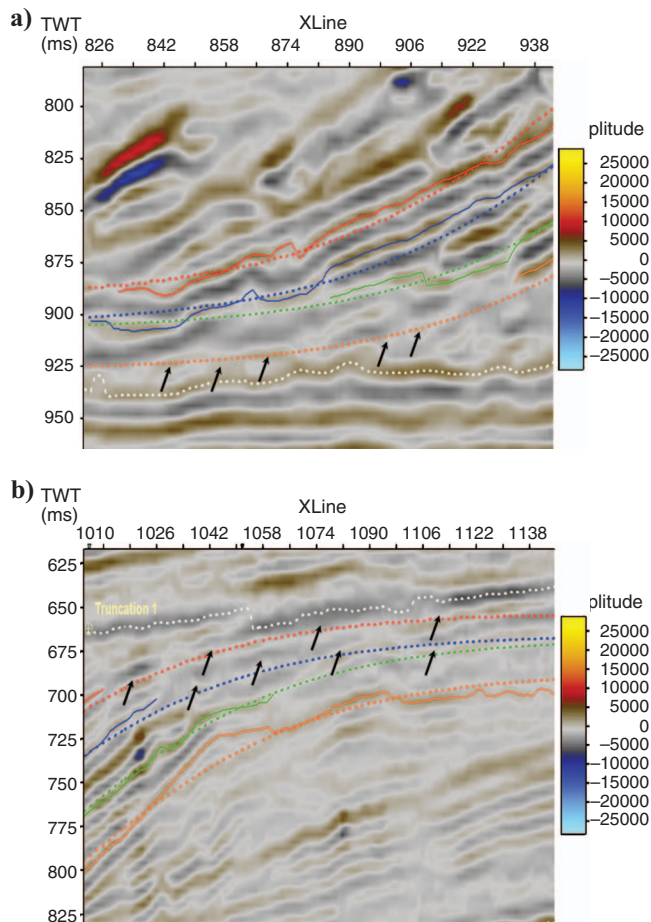


Figure 9. Enlarged versions of (a) the bottomset and (b) the topset of the clinoform indicated by the black rectangles in Figure 8. See text for discussion.

the geologic model, shale-rich sediments (higher impedance values) are deposited predominantly at the bottomset of the clinoform systems. Compaction usually causes deeper sediments to consolidate more than shallow ones; i.e., their impedance values increase. Both impedance models reveal that the sediments with higher impedance are indeed found at the bottom of the sequence (except for the part that was not modeled explicitly in method one, TWT 866–894 ms).

Moreover, an alternation of sand- and shale-rich sediments is observed in both impedance models, and they correlate well with each other.

Both methods have several limitations: they require poststack migrated seismic data, the availability of well data in the target zone, and a partial presence of clinoform structures at seismic scale (method one). Due to the absence of a second well in the area of interest, a blind test could not be applied to validate the methods.

For method one in the present work, only one specific geologic setting has been investigated, limiting a wider application of the results. However, a similar approach could be applied to characterize other systems, for instance, channelized reservoirs. The methodology to parameterize objects depends thus on the sedimentary environment of the data set, but it is scale, and to some extent shape, independent. The method has predictive capabilities. The estimated sigmoid parameters constitute a useful tool to characterize the changes in clinoform growth, which potentially could provide information

regarding fluctuations of sediment supply, long-term margin subsidence, and sea-level change.

For method two, there is no limitation in its application concerning the sedimentary environment of the data set because the structural information no longer is used explicitly.

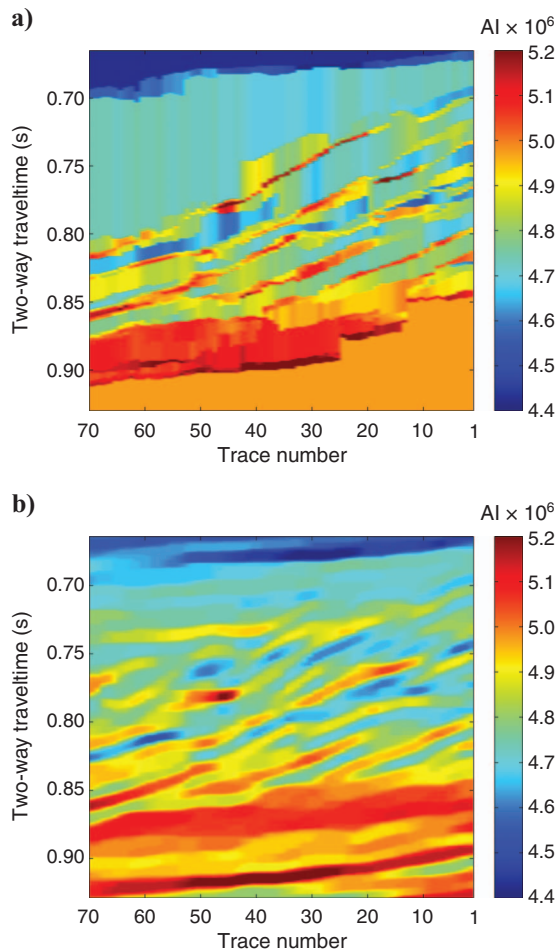


Figure 10. Resulting 2D impedance models of the clinoforms for (a) method one and (b) method two.

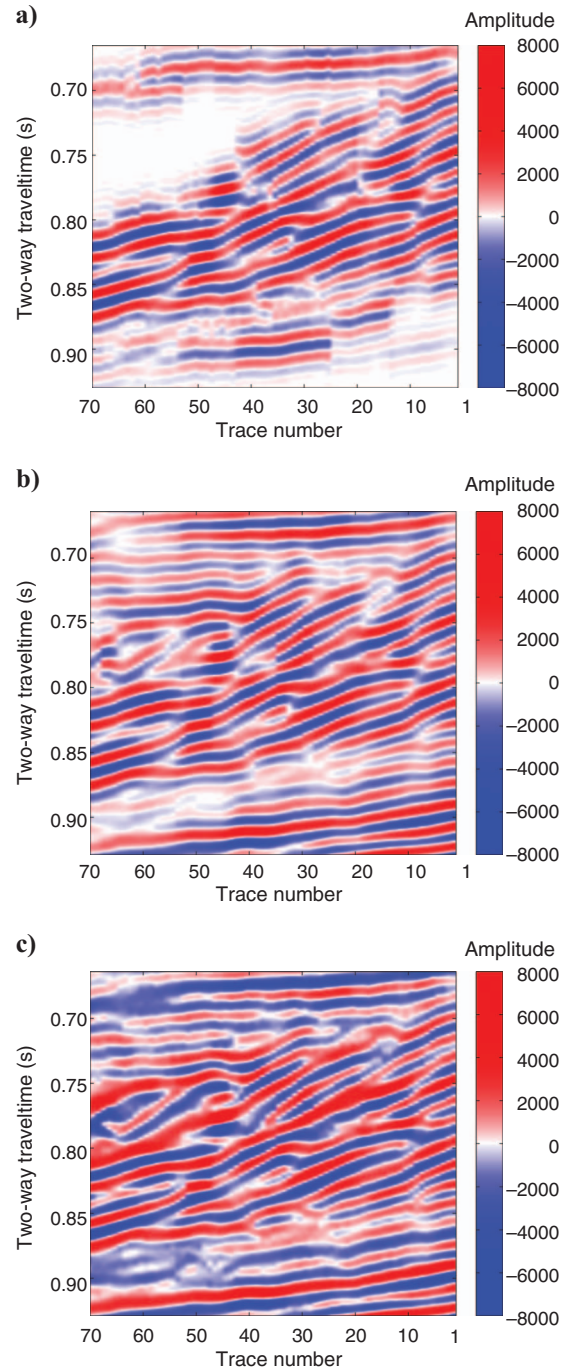


Figure 11. The simulated seismic sections based on the estimated impedance models of the clinoforms for (a) method one, (b) method two, and (c) the actual seismic.

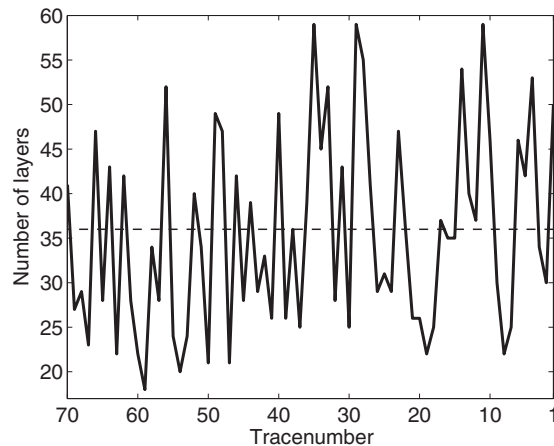


Figure 12. The number of identified layers in the target zone for the second method versus trace number.

CONCLUSIONS

The present study has resulted in two inversion methods that allow quantitative characterization of a fluvio-deltaic clinoform sequence. We used a trace-based deterministic inversion technique to solve this problem. The choice for deterministic inversion was motivated equally by the possibility of including structural information regarding the clinoform shapes into the inversion process. The integration of seismic data, well data, and geologic knowledge of the reservoir architecture allowed us to construct 2D geologic models of the subsurface. We chose acoustic impedance as a characterization property because it can be linked directly to reservoir properties such as porosity and, in some instances, fluid saturation. Because acoustic impedance is a layer property, impedance models are useful to geophysicists, petrophysicists, geologists, and engineers.

Both seismic inversion methods presented here show encouraging results when applied to a clinoform sequence from the North Sea. The results demonstrate a good match with the measured seismic data and well information. The methods are consistent with the initial models (well log), are constrained by it, and yet are flexible enough to detect deviations from the models, which are dictated by seismic data and due to changes in the geologic settings of the reservoir. The resulting impedance models of the clinoform show sharp transitions between internal layers.

The novelty of method one lies in the combination of the deterministic inversion method, which uses data-independent a priori information, thereby largely limiting the solution space and 2D geologic object parameterization with a limited number of parameters. The sigmoid models were used to steer the 1D trace inversion along the fluvio-deltaic sequence. Moreover, the sigmoid models provide sufficient well data extrapolation along the fluvio-deltaic sequence and assist in its characterization. The method allows lateral changes in impedance properties along the clinoform sequence and can parameterize the system geometry with a small number of parameters. Moreover, the method can extrapolate and align the disconnected events of parts of the geologic layers, which are at subsurface scale and cannot be tracked on the clinoform curve of the seismic image. In addition, a sharp inversion response was obtained.

Both proposed inversion methods are not fully two-dimensional but are more than a series of independently processed 1D inversions. Although it is trivial to rewrite the method as true 2D inversion, we

choose to implement it as a recursive series of 1D inversions to reduce the computational costs substantially. To stress the enforced continuity along the geologic structure, we call it pseudo-2D inversion.

The innovation of method two is that the objective function was modified by adding vertical and horizontal operators, which favor a sparse inversion solution and continuity of the inversion results along the sequence. The latter is responsible for the extrapolation of well data from trace to trace. The method differs from the well-known constrained sparse-spike acoustic inversion in the sparsity promoting factor used. We used a total variation criterion, which provides excellent constraints (a priori knowledge) for problems with sparse solutions, and introduced the hyperbolic norm that allowed us to use the Levenberg-Marquardt optimization method.

ACKNOWLEDGMENTS

The authors acknowledge the research center Delft Earth and Station for sponsoring this research. We also acknowledge the reviewers and the associate editor for their useful comments.

REFERENCES

- Alliney, S., and S. Ruzinsky, 1994, An algorithm for the minimization of mixed l_1 and l_2 norms with application to Bayesian estimation: *IEEE Transactions on Signal Processing*, **42**, 618–627.
- Aminzadeh, F., and P. de Groot, 2006, Neural networks and other soft computing techniques with applications in the oil industry: EAGE Publications BV.
- Amundsen, L., 1991, Comparison of the least-squares criterion and the Cauchy criterion in frequency-wavenumber inversion: *Geophysics*, **56**, 2027–2035, doi: 10.1190/1.1443015.
- Bosch, M., C. Carvajal, J. Rodrigues, A. Torres, M. Aldana, and J. Sierra, 2009, Petrophysical seismic inversion conditioned to well-log data: Methods and application to a gas reservoir: *Geophysics*, **74**, no. 2, O1–O15, doi: 10.1190/1.3043796.
- Cary, P. W., and C. H. Chapman, 1988, Automatic 1-D waveform inversion of marine seismic refraction data: *Geophysical Journal International*, **93**, no. 3, 527–546, doi: 10.1111/j.1365-246X.1988.tb03879.x.
- Cattaneo, A., F. Trincardi, A. Correggiari, and D. Carra, 2003, Clinoform construction in subaqueous deltas: An example from the Adriatic Sea (Italy): EGS-AGU-EUG Joint Assembly, Abstract No. 11277.
- Cattaneo, A., F. Trincardi, L. Langone, A. Asioli, and P. Puig, 2004, Clinoform generation on Mediterranean margins: *Oceanography*, **17**, 104–117.
- Cruse, E., A. Pica, M. Noble, J. McDonald, and A. Tarantola, 1990, Robust elastic nonlinear waveform inversion: Application to real data: *Geophysics*, **55**, 527–538, doi: 10.1190/1.1442864.
- Debye, H. W. J., and P. van Riel, 1999, l_p -norm deconvolution: *Geophysical Prospecting*, **38**, 381–403.
- Duijndam, A. J. W., 1988a, Bayesian estimation in seismic inversion: Part 1 — Principles: *Geophysical Prospecting*, **36**, no. 8, 878–898, doi: 10.1111/j.1365-2478.1988.tb02198.x.
- , 1988b, Bayesian estimation in seismic inversion: Part 2 — Uncertainty analysis: *Geophysical Prospecting*, **36**, no. 8, 899–918, doi: 10.1111/j.1365-2478.1988.tb02199.x.
- Emery, D., and K. Myers, 1996, *Sequence stratigraphy*: Wiley-Blackwell.
- Farsiu, S., M. D. Robinson, M. Elad, and P. Milanfar, 2004, Fast and robust multiframe super resolution: *IEEE Transactions on Image Processing*, **13**, no. 10, 1327–1344, doi: 10.1109/TIP.2004.834669.
- Gregersen, U., 1997, *Sequence stratigraphic analysis of Upper Cenozoic deposits in the North Sea based on conventional and 3-D seismic data and well-logs*: Ph.D. thesis, University of Aarhus.
- Huber, P., 1981, *Robust statistics*: Wiley.
- Li, Y., and F. Santosa, 1996, A computational algorithm for minimizing total variation in image restoration: *IEEE Transactions on Image Processing*, **5**, no. 6, 987–995, doi: 10.1109/83.503914.
- Luthi, S. M., 2001, *Geological well logs: Their use in reservoir modeling*: Springer-Verlag.
- Merletti, G. D., and C. Torres-Verdin, 2006, Accurate detection and spatial delineation of thin-sand sedimentary sequences via joint stochastic inversion of well logs and 3D pre-stack seismic amplitude data: Annual Technical Conference and Exhibition, SPE, Paper No. 102444.
- Moré, J. J., 1978, *The Levenberg-Marquardt algorithm: Implementation and*

- theory, in G. Watson, ed., *Lecture notes in mathematics*, vol. 630: Springer-Verlag, 105–116.
- Pendrel, J., 2001, Seismic inversion — The best tool for reservoir characterization: *CSEG Recorder*, **26**, 16–24.
- Pendrel, J., and P. van Riel, 1997, Methodology for seismic inversion and modeling: A western Canadian reef example: *CSEG Recorder*, **25**, 5–15.
- , 2000, Effect of well control on constrained sparse spike seismic inversion: *CSEG Recorder*, **25**, 18–26.
- Rudin, L. I., S. Osher, and E. Fatemi, 1992, Nonlinear total variation based noise removal algorithms: *Physica D: Nonlinear Phenomena*, **60**, no. 1–4, 259–268, doi: 10.1016/0167-2789(92)90242-F.
- Sørensen, J. C., U. Gregersen, M. Breiner, and O. Michelsen, 1997, High-frequency sequence stratigraphy of Upper Cenozoic deposits in the central and southeastern North Sea areas *Marine and Petroleum Geology*, **14**, no. 2, 99–123, doi: 10.1016/S0264-8172(96)00052-9.
- Steeghs, P., I. Overeem, and S. Tigrek, 2000, Seismic volume attribute analysis of the Cenozoic succession in the L08 block (Southern North Sea): *Global and Planetary Change*, **27**, no. what1–4, 245–262, doi: 10.1016/S0921-8181(01)00069-8.
- Tigrek, S., 1998, 3D seismic interpretation and attribute analysis of the L08 block, Southern North Sea Basin: Master's thesis, Delft University of Technology.
- Treitel, S., and L. Lines, 2001, Past, present, and future of geophysical inversion — A new millennium analysis: *Geophysics*, **66**, 21–24, doi: 10.1190/1.1444898.
- Van Eekeren, A. W. M., K. Schutte, and L. J. van Vliet, 2010, Multi-frame super-resolution reconstruction of small moving objects: *IEEE Transactions on Image Processing*, doi: 10.1109/TIP.2010.2068210.
- Van Riel, P., 2000, The past, present, and future of quantitative reservoir characterization: *The Leading Edge*, **19**, 878–881, doi: 10.1190/1.1438735.
- Van Riel, P., and P. R. Mesdag, 1988, Detailed interpretation of the North Sea Magnus field by integration of seismic and well information: 58th Annual International Meeting, SEG, Expanded Abstracts, 869–872, doi: 10.1190/1.1892413.